A new active asymmetry monitoring and control technique applied to critical aircraft flap control system failures

Applied Ocean Research 98 (2020) 102055

Contents lists available at ScienceDirect

Applied Ocean Research

journal homepage: www.elsevier.com/locate/apor

Parametric representation of arrays of wave energy converters for motion simulation and unknown input estimation: A moment-based approach

Nicolás Faedo*, Yerai Peña-Sanchez, John V. Ringwood

Centre for Ocean Energy Research, Maynooth University, Maynooth, Co. Kildare, Ireland

ARTICLE INFO

Keywords:
Radiation forces
Model order reduction
Moment-matching
Frequency-domain identification
WEC array
Unknown input estimation

ABSTRACT

When it comes to parameterisation of dynamical models for arrays of Wave Energy Converters (WECs), the most-used approach, within the wave energy literature, provides a state-space representation whose order (dimension) increases quadratically with the number of devices composing the WEC array. This represents a major drawback for key WEC design elements, such as motion simulation and unknown input estimation, being the latter essential to effectively maximise energy extraction from ocean waves. We present herein a multi-input, multi-output (MIMO) parameterisation strategy based on a system-theoretic interpretation of *moments*. The state-space representations computed with this moment-based approach *exactly* match the steady-state behavior of the target WEC system at specific (user-selected) interpolation points, providing efficient low dimensional models that can accurately represent the input-output dynamics of WEC arrays. Moreover, we show that there exists an intrinsic connection between wave excitation force estimation strategies and the moment-based parameterisation method proposed in this paper. We exploit this mathematical correlation to provide low order models that deliver the same degree of wave excitation force estimation accuracy to that obtained by implementing the currently-used parameterisation methods, with mild computational requirements. The performance of the strategy is analysed in terms of a case study, considering a WEC array composed of state-of-the-art CorPower-like devices, for both WEC motion simulation and wave excitation force estimation scenarios.

1. Introduction

Among the different renewable energy sources, wave energy has one of the highest power densities [1]. Despite being a vast resource, the cost involved in generating power from ocean waves is still prohibitive, compared to state-of-the-art wind or solar technologies [1]. To be precise, the current high installation, operation, maintenance, and decommissioning costs are hindering these novel wave energy extraction technologies from reaching a commercialisation stage. As a direct consequence of this, the roadmap towards successful commercialisation of Wave Energy Converters (WECs) naturally embodies the development of so-called WEC *arrays* or *farms*, which effectively incorporates several devices in a common sea area [2]. The devices composing a WEC farm are commonly installed in close proximity, mainly motivated by the underlying practical considerations, such as space limit, cable deployment, electricity delivery, and general maintenance.

Given that each WEC composing an array represents not only a wave absorber but also a wave generator [3, Chapter 8], the motion of each WEC is directly affected by the waves generated by adjacent devices (*i.e.* radiation effects). This feature further complicates the modelling task when compared to the case of a single device, often producing mathematical representations that are not tractable for key components facilitating the maximisation of energy absorption from ocean waves, such as real-time optimal controllers and wave excitation force estimators [4]. In light of this, at this development stage, modelling accurate but simple dynamical models is crucial for both the optimisation of the different components of each isolated WEC and layout of the array (*i.e.* optimal position of devices as a function of their hydrodynamic interactions), and the development of wave excitation force estimation strategies, which are essential in the design of optimal controllers that can maximise power conversion from ocean waves [4,5].

Boundary Element Methods (BEMs), readily available in up-to-date codes such as WAMIT or NEMOH [6], are the most commonly used methods to characterise the hydrodynamics of WECs. Nevertheless, the so-called hydrodynamic coefficients, obtained with these methods, are computed in the frequency-domain, characterising only the steady-state motion of the device under analysis. This represents a drawback for wave excitation force estimation strategies, which inherently require a time-domain representation of the WEC dynamics.

* Corresponding author.
E-mail address: nicolas.faedo@mu.ie (N. Faedo).

https://doi.org/10.1016/j.apor.2020.102055
Received 13 August 2019; Received in revised form 5 December 2019; Accepted 5 January 2020
Available online 13 April 2020

The motion of each floating device composing the WEC array can be expressed in the time-domain in terms of the well-known Cummins' equation [7], whose parameters can be computed from the frequency-domain hydrodynamic coefficients obtained by BEM solvers, following the theoretical framework presented in [8]. The resulting time-domain formulation is a Volterra integro-differential equation [9] which contains a convolution term accounting for the memory effects associated with radiation forces acting on the device. If we take into account that the WEC array is composed of $N \in \mathbb{N}$ devices, and that WECs (hydrodynamically) interact between each other due to radiation effects, the total number of convolution operation rises to N^2. In other words, a non-parametric impulse response function is required to model each cross-coupling term arising from radiation effects between devices.

The mere existence of these non-parametric convolution terms represent a drawback for most wave energy applications, including motion simulation and wave excitation force estimation theory perspectives. From a pure simulation point of view, it is well-known that the explicit computation of the convolution operator is computationally inefficient, often worsened by the necessity of a small (time) discretisation step to obtain accurate numerical integration.[1] Concerning modern state estimation techniques, they are virtually always based on the availability of a state-space description (*i.e.* a set of first-order differential equations) of the system under analysis [4].

Motivated by these aforementioned drawbacks, researchers often seek a parametric approximation of this radiation force subsystem in terms of a linear time-invariant representation, making explicit use of the hydrodynamic parameters computed with BEM-based codes. To be precise, the prevailing methodology is to approximate each of the radiation force-related convolution terms as a single-input single-output (SISO) system, even though the problem is inherently of a multiple-input multiple-output (MIMO) nature, as a consequence of the characteristics of the WEC array. Examples that consider this approach can be found in [5,11,12], among others. This so-called herein "multi-SISO" approach often leads to an unnecessarily high order parameterisation of the radiation force dynamics, leading to computationally inefficient representations. In fact, in this "multi-SISO" method each convolution operator is approximated with a parametric form of order $n_r \in \mathbb{N}$, yielding an input-output representation of the WEC array of order $2N + n_r N^2$. Though computationally more efficient than solving N^2 convolutions, the final dimension (order) of the WEC array model increases quadratically with N, potentially rendering any wave excitation force estimation strategy intractable for real-time energy-maximising control applications [4].

As discussed earlier in this section, the estimation of wave excitation force is a key element for the optimal extraction of energy from ocean waves. Explicitly, the determination of an optimal control force that maximises energy absorption always requires[2] knowledge of the instantaneous and future wave excitation force $\mathscr{F}_e$ acting on each WEC composing the array [4,13]. For a fixed body, $\mathscr{F}_e$ can be measured by integrating the pressure over the submerged body surface. This is certainly not the case when considering WECs, given that the wave excitation force is an unmeasurable quantity for a moving body, since the integrated pressure over the submerged WEC no longer represents $\mathscr{F}_e$ solely. To overcome this issue, several *unknown input* estimation strategies have been proposed within the wave energy literature. Particularly, the strategy presented in [5] has been proven to outperform state-of-the-art unknown input (observer) strategies applied in the wave energy field, both in terms of estimation accuracy and computational time [14]. This technique is based on optimal state estimation theory, and presents a combination of Kalman filtering [15] and the internal model principle[3] of control theory [16]. Note that, as highlighted previously, this estimation strategy requires a parameterisation of the input-output dynamics of the array in terms of a state-space representation, to successfully design a Kalman observer.

Following the roadmap towards successful WEC commercialisation, and the discussion offered in the previous paragraphs, the objective of this study is twofold. The model parameterisation problem for wave energy converter arrays is addressed first, proposing an extension of the SISO moment-matching-based identification framework developed in [17], for MIMO systems. Moment-based methods interpolate a certain number of points on the complex plane, termed *moments*, which are directly related to the frequency response of the target dynamical system under analysis. In fact, the transfer function of the approximating model obtained by this moment-based approach *exactly* matches the steady-state behavior of the target system at these specific interpolation points, which are user-selected. Secondly, and taking explicit advantage of the (frequency) interpolation feature of our moment-based strategy, the existence of an intrinsic connection between the wave excitation force estimation strategy presented in [5], and the moment-based parameterisation method proposed in this paper, is shown. This mathematical correlation can be exploited to compute exceptionally low-order models which provide the same degree of wave excitation force estimation accuracy as the currently implemented parameterisation methods, but with a significant improvement in terms of computational requirements. This has strong practical implications, being particularly appealing for real-time (combined) estimation and optimal control of wave energy farms, hence contributing to the roadmap towards successful commercialisation of WEC technologies. Note that a preliminary study on this subject was presented in [18]. This paper extends the results of [18], while also showing and exploiting the synergy between moments and the unknown input wave excitation force estimation problem. In addition, the application case is extended to a full-scale WEC array constituted by state-of-the-art heaving CorPower-like [19] devices.

The remainder of this paper is organised as follows. To keep this paper reasonably self-contained, Section 2 recalls key concepts behind the moment-matching framework for both SISO and MIMO systems. Section 3 presents the dynamics of a WEC array written in a suitable structure for the theoretical elements of this paper, while Section 4 presents a moment-based analysis of such a system. Section 5 proposes a moment-matching-based methodology to compute finite-order parametric models for the force-to-motion dynamics of the WEC array. Section 6 deals with a case study, for both motion simulation and wave excitation force estimation, explicitly showing the appealing characteristics of the moment-based parameterisation proposed in this paper. Finally, Section 7 encompasses the main conclusions of this study.

1.1. Notation and preliminaries

Standard notation is considered through this study, with any exceptions detailed in this section. $\mathbb{R}^+$ ($\mathbb{R}^-$) denotes the set of non-negative (non-positive) real numbers. $\mathbb{C}^0$ denotes the set of pure-imaginary complex numbers and $\mathbb{C}_{<0}$ denotes the set of complex numbers with a negative real part. The notation $\mathbb{N}_q$ indicates the set of all positive natural numbers up to q, *i.e.* $\mathbb{N}_q = \{1, 2, \cdots, q\}$. The symbol 0 stands for any zero element, dimensioned according to the context. The symbol $\mathbb{I}_n$ denotes the identity matrix of the space $\mathbb{C}^{n\times n}$. The spectrum of a matrix $A \in \mathbb{C}^{n\times n}$, *i.e.* the set of its eigenvalues, is denoted as $\lambda(A)$. The notation $W^\dagger$ with $W \in \mathbb{R}^{n\times m}$ denotes the *Moore-Penrose* inverse of W. The symbol

[1] Even though several algorithms have been proposed to alleviate the computational complexity associated to convolution operations, this still remains as an open topic [10].

[2] Note that there exist a number of suboptimal control implementations that only require instantaneous values of the excitation force (see [4]).

[3] Note that, as reported in [14], the combination of modern state-estimation strategies and the internal model principle has been exploited in several wave excitation force estimation studies, using a variety of state observers.

$\bigoplus$ denotes the direct sum of n matrices, *i.e.* $\bigoplus_{i=1}^{n} A_i = \mathrm{diag}(A_1, A_2, \cdots, A_n)$. The expression $\|X\|_F$, with $X \in \mathbb{C}^{n\times m}$ denotes the *Frobenius* norm of X. The *Kronecker product* between two matrices $M_1 \in \mathbb{R}^{n\times m}$ and $M_2 \in \mathbb{R}^{p\times q}$ is denoted as $M_1 \otimes M_2 \in \mathbb{R}^{np\times mq}$, while the *Kronecker delta* function is denoted as ${}_j^i\delta$. The convolution between two functions f and g over a set $\Omega \subset \mathbb{R}$, *i.e.* $\int_\Omega f(\tau)g(t-\tau)d\tau$ is denoted as $f{*}g$. The Fourier transform of a function $f \in L^2(\mathbb{R})$ is denoted by $\mathscr{F}\{f\}$, where $L^2(\mathbb{R}) = \{f\colon \mathbb{R} \to \mathbb{C} \mid \int_{\mathbb{R}} |f(x)^2| dx < \infty\}$. The symbol $e_{ij}^q \in \mathbb{R}^{q\times q}$ denotes a matrix with 1 in the ij-entry and 0 elsewhere. Finally, the symbol $\varepsilon_n \in \mathbb{R}^n$ denotes a vector with odd components equal to 1 and even components equal to 0.

In the remainder of this section, the formal definitions of two important operators are presented, since their definition in the literature can often be ambiguous.

Definition 1. [20] (Kronecker sum) The *Kronecker sum* between two matrices P_1 and P_2, with $P_1 \in \mathbb{R}^{n\times n}$ and $P_2 \in \mathbb{R}^{k\times k}$, is defined (and denoted) as

$$P_1 \hat{\oplus} P_2 \triangleq P_1 \otimes \mathbb{I}_k + \mathbb{I}_n \otimes P_2. \tag{1}$$

Definition 2. [20] (Vec operator) Given a matrix $P = [p_1, p_2, \cdots, p_m] \in \mathbb{R}^{n\times m}$, where $p_j \in \mathbb{R}^n$ with $j \in \mathbb{N}_m$, the vector valued operator *vec* is defined as

$$\mathrm{vec}\{P\} \triangleq \begin{bmatrix} p_1 \\ p_2 \\ \vdots \\ p_m \end{bmatrix} \in \mathbb{R}^{nm}. \tag{2}$$

2. Moment-based theory

With the final aim of keeping this paper reasonably self-contained, we briefly recall some of the key concepts behind the moment-matching framework, as developed in studies such as [21–23], for both SISO and MIMO systems. In particular, we make a special emphasis on the formal definition of *moment*, using a system-theoretic approach. Note that the formalism behind moments has been originally proposed within the field of model order reduction, being adapted for the wave energy parameterisation case in [17].

2.1. Moments for SISO systems

Consider a finite-dimensional, SISO, continuous-time system described, for $t \in \mathbb{R}^+$, by the state-space model[4]

$$\begin{aligned} \dot{x} &= Ax + Bu, \\ y &= Cx, \end{aligned} \tag{3}$$

where $x(t) \in \mathbb{R}^n$, $u(t) \in \mathbb{R}$, $y(t) \in \mathbb{R}$, $A \in \mathbb{R}^{n\times n}$, $B \in \mathbb{R}^n$ and $C^\intercal \in \mathbb{R}^n$. Consider the associated transfer function $W(s) = C(s\mathbb{I}_n - A)^{-1}B\colon \mathbb{C} \to \mathbb{C}$ and assume that (3) is minimal (*i.e* controllable and observable).

Definition 3. [24] The k-moment of system (3) at $s_i \in \mathbb{C}\backslash\lambda(A)$ is the complex number

$$\eta_k(s_i) = \frac{(-1)^k}{k!}\left[\frac{d^k}{ds^k}W(s)\right]_{s=s_i}, \tag{4}$$

with $k \geq 1$ integer.

Remark 1. Note that moments, as in Definition 3, are the coefficients of the Laurent expansion of the transfer function $W(s)$ about the complex point s_i.

[4] From now on, we drop the dependence on t when it's clear from the context.

The idea of the moment-based model order reduction technique is based on interpolating the transfer function of the original system (and the derivatives of this) and the transfer function of the reduced-order model (and the derivatives of this) at these specific interpolation points s_i.

One of the key results behind this framework is developed in [21], where the moments of system (3) are shown to be in a one-to-one relation with the steady-state response (provided it exists) of the output of the interconnection between a signal generator (sometimes referred to as exogenous system [25]) and system (3).

Lemma 1 ([21,22]). *Consider system (3) and the autonomous signal generator*

$$\begin{aligned} \dot{\xi} &= S\xi, \\ u &= L\xi, \end{aligned} \tag{5}$$

with $\xi(t) \in \mathbb{R}^\nu$, $S \in \mathbb{R}^{\nu\times\nu}$, $L^\intercal \in \mathbb{R}^\nu$ and $\xi(0) \in \mathbb{R}^\nu$. Assume that the triple (L, S, $\xi(0)$) is minimal, $\lambda(A) \subset \mathbb{C}_{<0}$, $\lambda(S) \subset \mathbb{C}^0$, and the eigenvalues of S are simple. Let $\Pi \in \mathbb{R}^{n\times\nu}$ be the (unique) solution of the Sylvester equation

$$A\Pi + BL = \Pi S. \tag{6}$$

Then, there exists a one-to-one relation between the moments $\eta_0(s_1)$, $\eta_0(s_2)$, $\cdots$, $\eta_0(s_\nu)$, with $s_i \in \lambda(S)$ for all $i \in \mathbb{N}_\nu$, and the steady-state response $C\Pi\xi$ of the output y of the interconnection of system (3) with the signal generator (5) (as in Fig. 1). In fact, the moments are uniquely determined by the matrix $C\Pi$.

Remark 2. The minimality of the triple (*L, S,* $\xi(0)$) implies the observability of the pair (*L, S*) and the *excitability*[5] of the pair (*S,* $\xi(0)$).

Remark 3. From now on, we refer to the matrix $C\Pi \equiv \underline{Y}$ as the *moment-domain equivalent* of y.

2.2. Moments for MIMO systems

Consider a finite-dimensional, MIMO, continuous-time system described, for $t \in \mathbb{R}^+$, by the state-space model

$$\begin{aligned} \dot{x} &= Ax + Bu, \\ y &= Cx, \end{aligned} \tag{7}$$

with[6] $x(t) \in \mathbb{R}^n$, $u(t) \in \mathbb{R}^q$, $y(t) \in \mathbb{R}^q$, $A \in \mathbb{R}^{n\times n}$, $B \in \mathbb{R}^{n\times q}$ and $C \in \mathbb{R}^{q\times n}$. Consider the associated transfer function $W(s) = C(s\mathbb{I}_n - A)^{-1}B\colon \mathbb{C} \to \mathbb{C}^{q\times q}$ and assume that (7) is minimal.

We now recall an adaptation of Lemma 1 for the MIMO case, which shows an explicit connection with the signal generator defined for the SISO case (5), in terms of the operator S.

Lemma 2 ([13]). *Consider system (7) and the autonomous multiple-output signal generator*

$$\begin{aligned} \dot{\Xi} &= (\mathbb{I}_q \otimes S)\Xi, \\ u &= L\Xi, \end{aligned} \tag{8}$$

with $\Xi(t) \in \mathbb{R}^{q\nu}$, $L \in \mathbb{R}^{q\times q\nu}$, $\Xi(0) \in \mathbb{R}^{q\nu}$, S as in Lemma 1, $\lambda(A) \subset \mathbb{C}_{<0}$, and assume that the triple of matrices $(L, \mathbb{I}_q \otimes S, \Xi(0))$ is minimal. Let $\Pi \in \mathbb{R}^{n\times q\nu}$ be the (unique) solution of the Sylvester equation

$$A\Pi + BL = \Pi(\mathbb{I}_q \otimes S). \tag{9}$$

Then, there exists a one-to-one relation between the moments $\eta_0(s_1)$, $\eta_0(s_2)$, $\cdots$, $\eta_0(s_\nu)$, with $s_i \in \lambda(S)$ for all $i \in \mathbb{N}_\nu$, and the steady-state response $C\Pi\Xi$ of the output y of the interconnection of system (7) with the signal generator (8).

Remark 4. We note that the literature in moment-matching for the MIMO case utilises the so-called *tangential interpolation* framework [23].

[5] We refer the reader to [26] for the definition of excitability.

[6] We focus on square systems, aiming to simplify the notation.

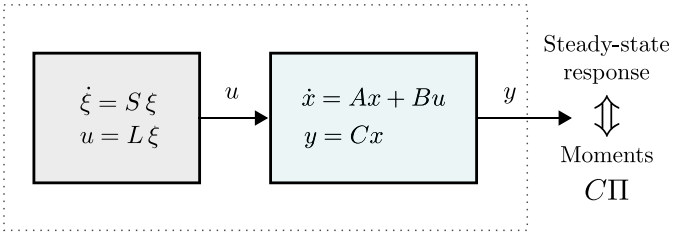

Fig. 1. Schematic of the interconnection between the system (3) and the signal generator (5) (adapted from [21]).

Herein, we are interested in retaining the exact same steady-state response for the WEC array, in spite of the consequent increase in model order with respect to the tangential approach. The rationality behind this argument stems from the fact that retaining an *exact* steady-state response in the parametric representation, greatly increases the accuracy of unknown input estimation procedures, as further discussed in Section 6.

Remark 5. Analogously to the SISO case, the moment for system (7) is computed in terms of the unique solution of a Sylvester equation, *i.e.* Eq. (9).

Based on this steady-state characterisation of moments, we recall the following key definition from [21,22], adapted for the MIMO case.

Definition 4. [21,22] Consider the signal generator (8). The system described by the equations

$$\begin{aligned} \dot{\Theta} &= F\,\Theta + G\,u, \\ \theta &= Q\,\Theta, \end{aligned} \tag{10}$$

with $\Theta(t) \in \mathbb{R}^{q\nu}$, $\theta(t) \in \mathbb{R}^{q}$, $F \in \mathbb{R}^{q\nu \times q\nu}$, $G \in \mathbb{R}^{q\nu \times q}$ and $Q \in \mathbb{R}^{q \times q\nu}$ is a model of system (7) at S if system (10) has the same moments at S as system (7).

Lemma 3 (*[21,22]*). *Consider system (7) and the signal generator (8). Then, the system (10) is a model of system (7) at S if*[7] $\lambda(F) \cap \lambda(S) = \emptyset$ *and*

$$\underline{Y} = QP, \tag{11}$$

where $\underline{Y} = C\Pi$ is the moment-domain equivalent of the output of system (7) computed from (9) and P is the unique solution of the Sylvester equation

$$FP + GL = P(\mathbb{I}_q \otimes S). \tag{12}$$

Remark 6. The steady-state output of the reduced order model (10) exactly matches the steady-state output of the system resulting from the interconnection of system (7) and the signal generator (8).

3. Governing motion equations for a WEC array

This section aims to introduce the basics behind linear modelling of arrays of wave energy converters in the time-domain, according to Cummins' equation [7]. The modelling assumptions considered herein are consistent across a wide variety of WEC applications presented in the literature, such as those concerning both WEC array estimation [5,11], and control studies [12,27,28], amongst others (the reader is referred to [4] for a comprehensive list of related studies and the modelling hypotheses considered).

3.1. Time-domain formulation

The equation of motion for an array of N wave energy converters can be expressed in time-domain according to Newton's second law, obtaining the hydrodynamic formulation [29],[3, Chapter 8]:

$$M\ddot{\chi} = \mathscr{F}_r + \mathscr{F}_h + \mathscr{F}_e - \mathscr{U}, \tag{13}$$

where $M = \bigoplus_{i=1}^{N} m_i$ is the mass matrix of the buoy with m_i the mass of the ith device, and each element of the vectors $\{\chi(t), \mathscr{F}_e(t), \mathscr{F}_h(t), \mathscr{F}_r(t)\} \subset \mathbb{R}^N$ contain the excursion $x_i\colon \mathbb{R}^+ \to \mathbb{R}$, the excitation force $f_{e_i}\colon \mathbb{R}^+ \to \mathbb{R}$, the hydrostatic restoring force f_{h_i} and the radiation force f_{r_i} acting on the ith device ($i \in \mathbb{N}_N$) of the array, respectively. The mapping $\mathscr{U}\colon \mathbb{R}^+ \to \mathbb{R}^N$ is composed of the PTO forces (*i.e.* potential control inputs) exerted on each device $u_i\colon \mathbb{R}^+ \to \mathbb{R}$.

The linearised hydrostatic force $\mathscr{F}_h$ can be written as $-S_h\chi$, where $S_h = \bigoplus_{i=1}^{N} s_{h_i}$ and each $s_{h_i} > 0$ denotes the hydrostatic stiffness of the ith WEC of the array. The radiation force $\mathscr{F}_r$ is modelled from linear potential theory and, using the well-known Cummins' equation [7], is

$$\mathscr{F}_r(t) = -\mu_\infty \ddot{\chi}(t) - \int_{\mathbb{R}^+} K(\tau)\dot{\chi}(t-\tau)d\tau, \tag{14}$$

where[8] $\mu_\infty = \lim_{\omega \to +\infty} A(\omega)$, $\mu_\infty > 0$ represents the added-mass matrix at infinite frequency and $K(t) = \sum_{i=1}^{N}\sum_{j=1}^{N} e_{ij}^N \otimes k_{ij}(t) \in \mathbb{R}^{N\times N}$, $k_{ij}\colon \mathbb{R}^+ \to \mathbb{R}$, $k_{ij} \in L^2(\mathbb{R})$, contains the (causal) radiation impulse response of each device (if $i = j$) and each interaction due to the radiated waves created by the motion of other devices (if $i \neq j$). Finally, the equation of motion of the WEC array can be expressed as

$$(M + \mu_\infty)\ddot{\chi} + K^*\dot{\chi} + S_h\chi = \mathscr{U}, \tag{15}$$

where the (total) external input $\mathscr{U}\colon \mathbb{R}^+ \to \mathbb{R}^N$ is composed of both the wave excitation force, and the control input, *i.e.* $\mathscr{U} = \mathscr{F}_e - \mathscr{U}$. The internal stability of Eq. (15), for the WEC case, has been analysed and guaranteed for any physically meaningful values of the parameters and the radiation mapping K involved, see [29].

Remark 7. We note that, if required by the application, a direct parameterisation of the control input can be used within this same framework, *i.e.* one can parameterise $\mathscr{U}$ [17,30] as

$$\mathscr{U} = M_u\ddot{\chi} + B_u\dot{\chi} + S_u\chi, \tag{16}$$

where $M_u = \bigoplus_{i=1}^{N} m_{u_i}$, $B_u = \bigoplus_{i=1}^{N} b_{u_i}$, $S_u = \bigoplus_{i=1}^{N} s_{u_i}$ and each value of the set $\{m_{u_i}, b_{u_i}, s_{u_i}\}_{i=1}^{N} \subset \mathbb{R}$ can be obtained using different optimal or suboptimal control strategies (see, for example, the strategies reported in [4]).

Remark 8. Though excluded in this paper (motivated by a large number of studies considering the same modelling assumptions discussed at the beginning of this section), linearised viscous forces [31] can also be included straightforwardly in Eq. (15). In addition, we note that nonlinear viscous effects can be accommodated within the parameterisation framework described in Section 5, by following [32].

3.2. Frequency-domain formulation

As discussed in Section 1, BEM solvers are widely considered in the literature to characterise (hydrodynamically) WEC devices, mainly due to their efficient computational performance, when compared to time-domain methods [33]. Given that these hydrodynamic codes provide a frequency-response charaterisation of the device under analysis, it is natural to regard the motion of the WEC array using a frequency-domain description. Applying the Fourier transform to (15), and considering the velocity of each device as measurable outputs *i.e.* the mapping $\dot{\chi}$, the following representation

$$\mathscr{F}\{\dot{\chi}\}(j\omega) = \mathscr{F}\{\mathscr{U}\}(j\omega)H(j\omega), \tag{17}$$

where $H\colon \mathbb{C}^0 \to \mathbb{C}^{N\times N}$ denotes the force-to-velocity frequency response mapping of the WEC array, holds. Note that the expression force-to-velocity (or more generally, force-to-motion) is used here to denote the frequency response of the WEC considering the total external force as the input to the system. $H(j\omega)$ can be computed as a function of a well-

[7] Note that $\lambda(\mathbb{I} \otimes A) = \lambda(A)$ for any matrix $A \in \mathbb{R}^{n\times n}$ [20].

[8] See Section 3.2 for the definition of $A(\omega)$.

known set of frequency-dependent parameters, Folley [3], Falnes [29] namely

$$H(j\omega) = \left(B(\omega) + j\omega A(\omega) + \frac{S_h}{j\omega}\right)^{-1}, \tag{18}$$

where $B(\omega)$ and $A(\omega)$ represent the radiation damping, and the radiation added mass matrix of the device, respectively. These frequency-dependent device parameters are virtually always calculated using hydrodynamic codes at a finite set of uniformly-spaced frequency samples $\Omega = \{\omega_i\}_{i=1}^{M}$ with $\Omega \subset [\omega_l,\ \omega_u]$, where ω_l and ω_u represents the lower and upper bound of the range, respectively. The selection of such a frequency range depends explicitly on the application, as discussed in [17].

4. Moment-based WEC array formulation

To consider the theoretical results recalled in Section 2 for this WEC array case, the equation of motion presented in (15) needs to be re-written in a more suitable structure. The following state-space representation, for the WEC array dynamics, is proposed:

$$\mathscr{H}: \begin{cases} \dot{\varphi} &= A_\varphi \varphi + B_\varphi \mathrm{u}, \\ y_\varphi &= C_\varphi \varphi = \dot{\chi}, \end{cases} \tag{19}$$

where $\varphi(t) = [\phi_1(t), \cdots, \phi_N(t)]^\intercal \in \mathbb{R}^{2N}$ is the state-vector of the continuous-time model, with $\phi_i = [x_i, \dot{x}_i]^\intercal$. The function $\mathrm{u}: \mathbb{R}^+ \to \mathbb{R}^N$, assumed to be the input of system (19), is defined as

$$\mathrm{u} = \mathscr{U} - K^* \dot{\chi}. \tag{20}$$

Under this assumption, the matrices in (19) can be written in compact form as follows:

$$\begin{aligned} A_\varphi &= \textstyle\sum_{i=1}^{N}\sum_{j=1}^{N} e_{ij}^N \otimes A_{\varphi_{ij}}, \quad B_\varphi = \sum_{i=1}^{N}\sum_{j=1}^{N} e_{ij}^N \otimes B_{\varphi_{ij}}, \\ C_\varphi &= \mathbb{I}_N \otimes [0\ 1], \end{aligned} \tag{21}$$

with each $A_{\varphi_{ij}} \in \mathbb{R}^{2\times 2}$, $B_{\varphi_{ij}} \in \mathbb{R}^2$ defined as

$$A_{\varphi_{ij}} = \begin{bmatrix} 0 & {}^{i}_{j}\delta \\ -\mathscr{M}_{ij} s_{h_i} & 0 \end{bmatrix}, \quad B_{\varphi_{ij}} = \begin{bmatrix} 0 \\ \mathscr{M}_{ij} \end{bmatrix} \tag{22}$$

where $\mathscr{M}_{ij}$ is the ijth element of the inverse generalised mass matrix $(M + \mu_\infty)^{-1}$.

Within the moment-based framework, the input mapping $\mathscr{U}$ (*i.e.* the total external force), is expressed as an autonomous multiple-output implicit form signal generator as

$$\begin{aligned} \dot{\Xi}_e &= (\mathbb{I}_N \otimes S)\Xi_e, \\ \mathscr{U} &= L_e \Xi_e, \end{aligned} \tag{23}$$

where the dimension of S is as in (8), $\Xi_e(t) \in \mathbb{R}^{N\nu}$, $L_e \in \mathbb{R}^{N\times N\nu}$ and, without loss of generality, the initial condition of the signal generator is chosen as $\Xi_e(0) = \varepsilon_{N\nu}$. Given the characteristics of $\lambda(S)$, we consider the finite set $\mathscr{F} = \{\omega_p\}_{p=1}^{f} \subset \mathbb{R}^+$ and write the matrix S in a real block-diagonal form as

$$S = \bigoplus_{p=1}^{f} \begin{bmatrix} 0 & \omega_p \\ -\omega_p & 0 \end{bmatrix}, \tag{24}$$

where $\nu = 2f$, $f > 0$ integer, and $\lambda(S) = (j\mathscr{F}) \cup (-j\mathscr{F})$.

Remark 9. With this selection of matrices, the assumption on the minimality of the triple $(L_e, \mathbb{I}_N \otimes S, \Xi_e(0))$ holds as long as the pair $(L_e, \mathbb{I}_N \otimes S)$ is observable.

Remark 10. Note that each ω_p in (24) represents a desired interpolation point for the model reduction process (see Remark 6), *i.e.* a frequency where the transfer function of the reduced-order model matches the transfer function of the original system.

Under this selection of matrices, the moments of system (19), driven by the signal generator (23), can be computed by solving a specific Sylvester equation (see Theorem 2). Such an equation can be specialised for the WEC array case as

$$A_\varphi \Pi_\varphi + B_\varphi(L_e - \underline{\mathscr{Y}}) = \Pi_\varphi(\mathbb{I}_N \otimes S), \tag{25}$$

where $\Pi_\varphi \in \mathbb{R}^{2N\times N\nu}$ and $\underline{\mathscr{Y}}$ is the moment-domain equivalent of the radiation matrix convolution term. The moment-domain equivalent of the velocity can be expressed in terms of the solution of (25) straightforwardly as $\underline{\mathscr{V}} = C_\varphi \Pi_\varphi$. Aiming to keep this paper reasonably self-contained, we recall the following lemma from [13], which defines the quantity $\underline{\mathscr{Y}}$.

Lemma 4 (*[13]*). *The moment-domain equivalent of the convolution integral in (14) can be computed as*

$$\underline{\mathscr{Y}} = \sum_{i=1}^{N}\sum_{j=1}^{N} e_{ij}^N \underline{\mathscr{V}}(\mathbb{I}_N \otimes \mathscr{R}_{ij}), \tag{26}$$

where each $\mathscr{R}_{ij} \in \mathbb{R}^{\nu\times\nu}$ is a block-diagonal matrix defined as

$$\mathscr{R}_{ij} = \bigoplus_{p=1}^{f} \begin{bmatrix} {}^{i}_{j}\mathscr{k}_{\omega_p} & {}^{i}_{j}\mathscr{m}_{\omega_p} \\ -{}^{i}_{j}\mathscr{m}_{\omega_p} & {}^{i}_{j}\mathscr{k}_{\omega_p} \end{bmatrix}, \tag{27}$$

with

$${}^{i}_{j}\mathscr{k}_{\omega_p} = B_{ij}(\omega_p) \quad {}^{i}_{j}\mathscr{m}_{\omega_p} = \omega_p \left[A_{ij}(\omega_p) - \mu_{\infty_{ij}}\right], \tag{28}$$

where $A_{ij}(\omega)$ is the added-mass matrix, $B_{ij}(\omega)$ is the radiation damping matrix of the device at each specific frequency induced by the eigenvalues of S, and $\mu_{\infty ij}$ is the ijth entry of the matrix μ_∞.

Following Lemma 4, we now present a compact result to directly compute $\underline{\mathscr{V}}$, by solving (25), with $\underline{\mathscr{Y}}$ defined as in (26).

Lemma 5. *Suppose system (19) is asymptotically stable in the Lyapunov sense. Then, the moment-domain equivalent of the output y_φ of system (19), i.e. $\underline{\mathscr{V}}$, can be uniquely computed as*

$$\mathrm{vec}\{\underline{\mathscr{V}}\} = (\mathbb{I}_N \otimes \Phi_\varphi^{\mathscr{R}})\mathrm{vec}\{L_e\}, \tag{29}$$

where the matrix $\Phi_\varphi^{\mathscr{R}} \in \mathbb{R}^{N\nu\times N\nu}$ is defined as

$$\begin{aligned} \Phi_\varphi^{\mathscr{R}} &= (\mathbb{I}_\nu \otimes C_\varphi)\Phi_\varphi^{-1}(\mathbb{I}_\nu \otimes -B_\varphi), \\ \Phi_\varphi &= (S \oplus^{\wedge} A_\varphi) + \textstyle\sum_{i=1}^{N}\sum_{j=1}^{N} \mathscr{R}_{ij}^\intercal \otimes -B_\varphi e_{ij}^N C_\varphi. \end{aligned} \tag{30}$$

Proof. The proof of this lemma follows from a direct application of the vec operator (as in Definition 2) to Eq. (25) and, hence, it is omitted. □

5. Parametric models achieving moment-matching

In this section, we pose an algorithm to compute an approximated parametric time-domain model of the input-output dynamics (force-to-motion) of the WEC array, based on the moment-domain representation of the N-device WEC array dynamics derived in Section 4. In particular, we consider the theoretical structure behind the family of systems (10) achieving moment-matching, in synergy with some of the main notions behind frequency-domain subspace-based identification methods, as proposed in [34] and briefly recalled in the subsequent paragraph.

Following the well-established theory on subspace-based methods reported in [34], both the dynamic and output matrix from system (19) can be approximated in terms of the singular value decomposition of the Hankel matrix $\hat{H}$, constructed[9] from the input-output frequency-domain data of the WEC array (18) computed at the finite set of

[9] We refer the reader to [34] for further details on the computation of the Hankel matrix $\hat{H}$.

uniformly spaced frequencies Ω (see Section 3.2). This α-dimensional approximated matrices ${}^{d}\hat{A}_{\alpha} \in \mathbb{R}^{\alpha\times\alpha}$, $\hat{C}_{\alpha} \in \mathbb{R}^{N\times\alpha}$ (where ${}^{d}\hat{A}_{\alpha}$ corresponds to a discrete-time model) can be computed [34] as

$$ {}^{d}\hat{A}_{\alpha} = (J_1\hat{U}_{\alpha})^{\dagger}J_2\hat{U}_{\alpha}, \quad \hat{C}_{\alpha} = J_3\hat{U}_{\alpha}, \tag{31} $$

where the singular value decomposition of the Hankel matrix is written as

$$ \hat{H} = [\hat{U}_{\alpha} \;\; \hat{U}_{o}] \begin{bmatrix} \hat{\Sigma}_{\alpha} & 0 \\ 0 & \hat{\Sigma}_{o} \end{bmatrix} \begin{bmatrix} \hat{V}_{\alpha}^{\intercal} \\ \hat{V}_{o}^{\intercal} \end{bmatrix}, \tag{32} $$

and the matrices $J_1, J_2 \in \mathbb{R}^{(N-1)N\times N^2}$, $J_3 \in \mathbb{R}^{N\times N^2}$ are defined as

$$ \begin{aligned} J_1 &= [\mathbb{I}_{(N-1)N} \;\; 0], \\ J_2 &= [0 \;\; \mathbb{I}_{(N-1)N}], \\ J_3 &= [\mathbb{I}_{N} \;\; 0]. \end{aligned} \tag{33} $$

Remark 11. Note that, with the knowledge of the frequency sampling associated to the set Ω, the continuous-time equivalent matrix $\hat{A}_{\alpha}$ can be computed directly from ${}^{d}\hat{A}_{\alpha}$ using, for instance, the bilinear (Tustin) mapping, as discussed in [34].

Remark 12. If ${}^{d}\hat{A}_{\alpha}$, computed as in (31), has unstable eigenvalues, one can always project such a set into the complex unit circle, following the procedure described in [34]. This guarantees the computation of a Jury matrix ${}^{d}\hat{A}_{\alpha}$, if required.

We are now ready to pose an algorithm to compute a moment-matching based model of the WEC array, exploiting the result of Proposition 5 and the system-theoretic structure of (10).

Algorithm 1 is based on the idea of building the parametric model $\tilde{\mathscr{H}}_{\mathscr{F}}$ matching the f (user-defined) frequencies of the set $\mathscr{F}$, exploiting the system structure of (10) and solving for an equality-constrained optimisation problem. Summarising, this optimisation process aims for the computation of the input matrix G_{φ}^{opt} that minimises the difference between the target frequency response and that of (10) (in terms of the matrix Euclidean norm) while guaranteeing the moment-matching conditions in the obtained parametric model. The optimisation problem of Algorithm 1 is a constrained least-squares problem and can be solved using computationally efficient state-of-the-art solvers as those detailed in, for example, Boyd and Vandenberghe [35].

Remark 13. The model computed with Algorithm 1 has dimension $N\nu$ with $\nu = 2f$, where N is the number of devices in the WEC array and f is the number of interpolation points (frequencies) selected in the set $\mathscr{F}$. This is a consequence of the fact that, for each frequency ω_i and each device, both $\pm j\omega_i$ are chosen as eigenvalues of the real-valued matrix $\mathbb{I}_N \otimes S$.

Remark 14. The notation $\tilde{\mathscr{H}}_{\mathscr{F}}$ refers to an approximated parametric time-domain model of the force-to-velocity dynamics of the device under analysis $\mathscr{H}$ in (19), by matching the frequencies selected in the set $\mathscr{F}$ using the procedure described in Algorithm 1.

6. Case study: array of CorPower-like devices

This section presents an application case to illustrate and analyse the proposed strategy, based on the square WEC array layout studied in [5], and depicted herein in Fig. 2. This particular layout is composed of $N = 4$ energy converters, where each of the four devices composing the WEC farm is a state-of-the-art full-scale CorPower[10]-like device oscillating in heave (translational motion). Note that this type of device is often considered as a case study due to its intrinsic geometrical complexity (see, for example, Giorgi and Ringwood [36]), and is illustrated herein in Fig. 3, along with its corresponding physical dimensions specified in metres. These dimensions are based on the experimental study performed in [37]. From now on, and without any loss of generality, we set the control input $\mathscr{U} = 0$, *i.e.* $\mathscr{U} = \mathscr{F}_e$ in Eq. (15).

To fully characterise this farm, Fig. 4 presents the hydrodynamic characteristics of the WEC array considered in this application case, in terms of its corresponding radiation damping and radiation added-mass matrices, *i.e.* $B(\omega)$ and $A(\omega)$, respectively.[11] Note that, since the devices composing the WEC farm are identical (*i.e.* CorPower-like devices), the corresponding hydrodynamic characteristics (including interactions arising due to radiation effects) present symmetrical behavior, in accordance to the layout depicted in Fig. 2. That said, only three elements of the matrices $\{B(\omega), A(\omega)\} \subset \mathbb{R}^{4\times4}$ are required to completely characterise the hydrodynamic parameters of the complete array. These are plotted in Fig. 4, along with the corresponding symmetry pattern[12] for both matrices $A(\omega)$ and $B(\omega)$. Note that we compute these hydrodynamic coefficients using BEM codes at a finite set of frequencies with $\omega_u = 3$ [rad/s]. This is motivated by the fact that ocean wave peak periods typically lie between 3 [s] and 16 [s], which implies that the frequency range that characterises the wave excitation force $\mathscr{F}_e$ is approximately [0.4,2.1] [rad/s].

For both the numerical device motion, and wave excitation force estimation analysis of this section, we consider irregular waves as inputs, with a Spectral Density Function (SDF) computed according to the Joint North Sea Wave Observation Project (JONSWAP) [39] and with a peak period $T_p = 7.5$ [s], significant wave height H_s in the set {1.5, 2, 3} [m] and peak enhancement factor $\gamma = 3.3$ (shown in Fig. 5). The total duration of each generated wave and, hence, each simulation, is set to 200 [s]. Finally, without any loss of generality, the incident wave direction β is set to $\beta = 0$ (see Fig. 2).

As anticipated in Section 5, we consider the proposed moment-matching-based strategy for both WEC motion simulation (in the frequency- and time-domains) and wave excitation force estimation (time-domain). In order to obtain statistically meaningful and consistent results for the time-domain scenarios, and since the waves are generated from sets of random amplitudes [40], it is found that the mean of 15 simulations is necessary to obtain a 95% confidence interval with a half-width of 0.2% of the mean, computed as in [5].

From now on, we denote the frequency-domain model corresponding to the WEC array $H(j\omega)$ as the *target* frequency-domain response. In addition, we use the notation $H_{ij}(j\omega)$ for the ijth element of the matrix $H(j\omega)$. More precisely, H_{ij}: $\mathbb{C}^0 \longrightarrow \mathbb{C}$ is the frequency response mapping between the wave excitation force acting on the ith device f_{e_i}, and the output velocity of the jth device $\dot{x}_j$.

6.1. WEC array motion simulation

Following the theoretical results developed in Section 4 and the method proposed in Algorithm 1, we now proceed to the explicit computation of a moment-based parametric model $\tilde{\mathscr{H}}_{\mathscr{F}}$ to approximate the force-to-velocity dynamics $\mathscr{H}$ described in Eq. (19). To fulfill this objective, we make explicit use of the target frequency response operator $H(j\omega)$ computed using BEM codes. We recall that a key feature of this moment-based strategy is that the user is allowed to select a set of frequencies $\mathscr{F}$ to interpolate, *i.e.* a set of frequency points where the approximating model $\tilde{\mathscr{H}}_{\mathscr{F}}$ *exactly* matches the steady-state response of $\mathscr{H}$ in (19).

As discussed in [17] for the SISO case (*i.e.* single device in the array), a sensible selection of the interpolation set can be achieved by

[10] See [19] for up-to-date detail on this device.

[11] For this study, the hydrodynamic characteristics of the WEC array are computed using the BEM software NEMOH [6].

[12] The reader is referred to [38, Chapter 8] for an extensive discussion on the hydrodynamic coefficients of WEC arrays and the principles behind this symmetrical behaviour.

1 Select a set of f interpolation points (frequencies) $\mathscr{F} = \{\omega_p\}_{p=1}^{f} \subset \mathbb{R}^+$ to achieve moment-matching.

2 Compute the matrix $\mathbb{I}_N \otimes S$ following (24) and select any L_e such that the pair $(L_e, \mathbb{I}_N \otimes S)$ is observable.

3 Calculate the moment-domain equivalent of the output of system (19) $\underline{\mathcal{V}}$ using the result of Lemma 5.

4 Compute the matrices $\hat{A}_{N\nu}$ and $\hat{C}_{N\nu}$ as described in equation (31).

5 Consider the familiy of systems (10) and set $F = F_\varphi = \hat{A}_{N\nu}$ and $Q = Q_\varphi = \hat{C}_{N\nu}$.

6 Consider the frequency response of (10) as a function of G_φ *i.e.*

$$\tilde{H}_{\mathscr{F}}(j\omega, G_\varphi) = Q_\varphi\big(j\omega - F_\varphi\big)^{-1} G_\varphi.$$

Using the frequency set $\Omega = \{\omega_i\}_{i=1}^{M}$, compute the input matrix G_φ^{opt} with the following optimisation-based procedure:

$$\begin{aligned}
&G_\varphi^{\text{opt}} = \arg\min_{G_\varphi} \textstyle\sum_{i=1}^{M} \left\| \tilde{H}_{\mathscr{F}}(j\omega_i, G_\varphi) - H(j\omega_i) \right\|_F^2 \\
&\text{subject to:} \\
&F_\varphi P_\varphi + G_\varphi L_e = P_\varphi(\mathbb{I}_N \otimes S), \\
&Q_\varphi P_\varphi = \underline{\mathcal{V}}.
\end{aligned}$$

7 Compute a $N\nu$-dimensional WEC array time-domain model achieving moment-matching at S from (10) as

$$\tilde{\mathcal{H}}_{\mathscr{F}} : \begin{cases} \dot{\Theta}_\varphi &= F_\varphi \Theta_\varphi + G_\varphi^{\text{opt}} \mathscr{U}, \\ \theta_\varphi &= Q_\varphi \Theta_\varphi. \end{cases}$$

Algorithm 1. Moment-matching-based parameterisation WEC array model.

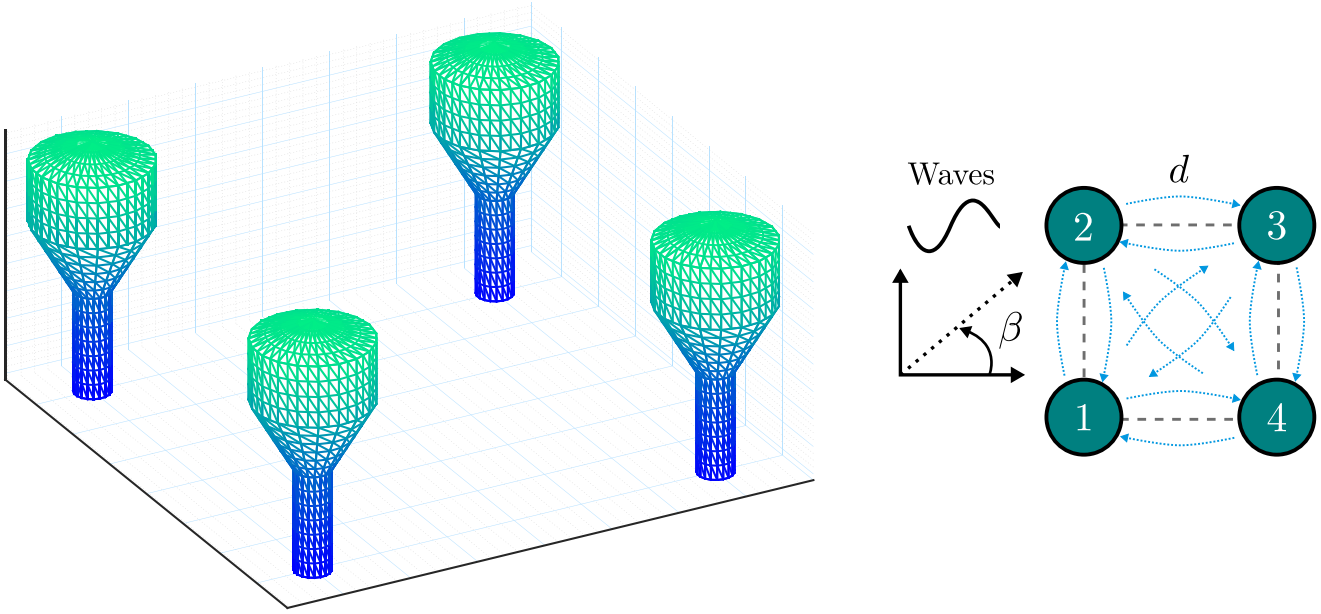

Fig. 2. Schematic and dimensions of the CorPower-like device as studied in [36,37] (dimensions are in metres).

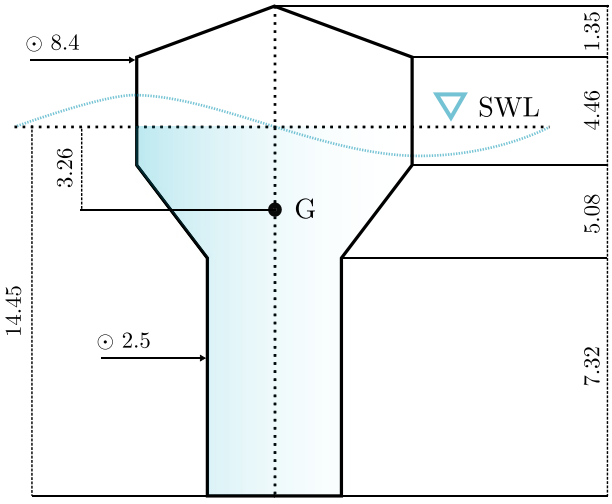

Fig. 3. Hydrodynamic characteristics of the CorPower-like WEC farm, in terms of the matrices $B(\omega)$ (solid, left axis) and $A(\omega)$ (dashed, right axis). Note that there is a one-to-one relation between the colors of the lines and the corresponding symmetry pattern depicted in the figure.

analysing the gain of the target frequency response, and selecting points that characterise dynamically important features of the WEC. By way of example, a sensible selection always includes the resonant frequency of the device under analysis. We note that this is the frequency where the maximum amplification occurs, *i.e.* the frequency characterising the $\mathscr{H}_\infty$-norm of the WEC system. For this MIMO case, it is well-known that the system gain depends intrinsically on the corresponding input direction [41], hence the selection of these dynamically relevant points cannot be done by simply inspecting each $H_{ij}(j\omega)$ individually. As a matter of fact, the gain of a MIMO system is defined in terms of the *singular values* of $H(j\omega)$, plotted, for our CorPower-array case, in Fig. 6 (dashed-blue).

Based on the previous discussion, and to test the proposed strategy in the motion (velocity) simulation case, we consider different frequency interpolation points sets $\mathscr{F}$, as follows:

- $\mathscr{F}_1^{\text{sim}} = \{1.17\}$,
- $\mathscr{F}_2^{\text{sim}} = \{1.17,\ 1.11\}$,
- $\mathscr{F}_3^{\text{sim}} = \{1.17,\ 1.11,\ 1.8\}$,
- $\mathscr{F}_4^{\text{sim}} = \{1.17,\ 1.11,\ 1.8,\ 0.6\}$.

Note that $\mathscr{F}_i^{\text{sim}} \subset \mathscr{F}_j^{\text{sim}}$ for $i < j$, with $\{i, j\} \in \mathbb{N}_4$. As can be appreciated from Fig. 6, the set $\mathscr{F}_1^{\text{sim}}$ includes a key interpolation point, which explicitly characterises the $\mathscr{H}_\infty$-norm of the WEC array. To be precise, the presented moment-based strategy is able to preserve the $\mathscr{H}_\infty$-norm of the target system by simply including the corresponding frequency in the interpolation set. The set $\mathscr{F}_2^{\text{sim}}$ additionally includes the frequency point where the second maximum amplification peak occurs. Finally, the sets $\mathscr{F}_3^{\text{sim}}$ and $\mathscr{F}_4^{\text{sim}}$ expand $\mathscr{F}_2^{\text{sim}}$ by including a low-, and a low- and high- frequency component, respectively.

We begin the assesment of the moment-based parameterisation approach in terms of WEC array motion simulation, by illustrating the performance of the approximating models $\tilde{\mathscr{H}}_{\mathscr{F}_1^{\text{sim}}}$ and $\tilde{\mathscr{H}}_{\mathscr{F}_4^{\text{sim}}}$. Fig. 6 presents the so-called *sigma-values* plot, for both the target response $H(j\omega)$ (dashed-blue), and the approximating frequency response mappings (solid-green) $\tilde{H}_{\mathscr{F}_1^{\text{sim}}}$ (top) and $\tilde{H}_{\mathscr{F}_4^{\text{sim}}}$ (bottom). The interpolation points selected for the computation of each approximating parametric structure are denoted by an empty black circle. Note that, as expected by the theoretical foundations of this moment-based strategy, the approximating models have *exactly* the same gain as the target model $H(j\omega)$ of the WEC array, for each element of the corresponding interpolation set $\mathscr{F}^{\text{sim}}$. In addition, it can be readily appreciated that, by a sensible selection of the interpolation frequency set $\mathscr{F}_1^{\text{sim}}$, the model $\tilde{\mathscr{H}}_{\mathscr{F}_1^{\text{sim}}}$, *i.e.* a parametric description computed using a single interpolation point, already provides an accurate frequency-domain description when compared with the target steady-state response of the WEC array under study. Though considering $\mathscr{F}_1^{\text{sim}}$ as an interpolation set provides quite accurate results, the decrease in the overall approximation error from system $\tilde{\mathscr{H}}_{\mathscr{F}_1^{\text{sim}}}$ to $\tilde{\mathscr{H}}_{\mathscr{F}_4^{\text{sim}}}$ can be clearly appreciated (further discussed in Table 1).

As a conclusive graphical illustration of the frequency-domain performance for the models computed via this moment-based strategy, Fig. 7 presents the Bode diagrams for the mappings $H_{11}(j\omega)$, $H_{12}(j\omega)$ and $H_{14}(j\omega)$. Note that, due to the underlying symmetry of the WEC array illustrated in Fig. 4, these mappings are indeed sufficient to completely characterise the frequency response function $H(j\omega)$. Analogously to what is presented in Fig. 6, Fig. 7 uses the same colors and lines to characterise the target response, and the approximating models $\tilde{H}_{\mathscr{F}_1^{\text{sim}}}$ (top) and $\tilde{H}_{\mathscr{F}_4^{\text{sim}}}$ (bottom). Once again, it can be appreciated that, by a

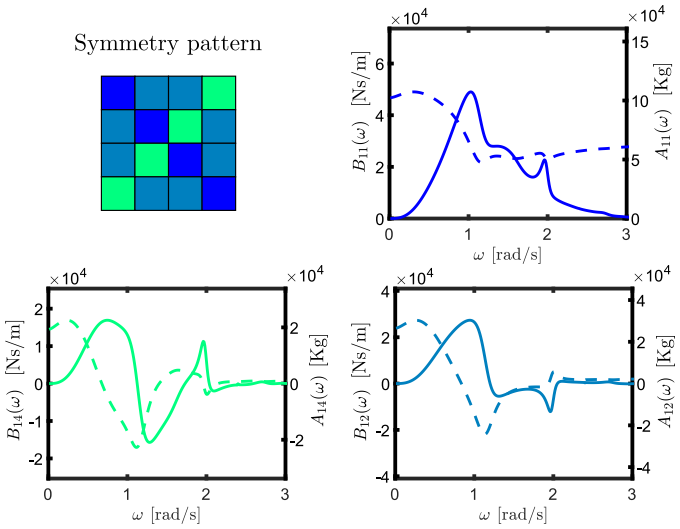

Fig. 4. Regular-polytope-type WEC array layout considered for the application case. The distance d between devices is set to twice the diamater of the upper part of the float, *i.e.* $d \approx 17$ [m]. The dotted-blue arrows represent the hydrodynamic interaction between WECs in the array, while β denotes the incident wave direction. (For interpretation of the references to color in this figure legend, the reader is referred to the web version of this article.)

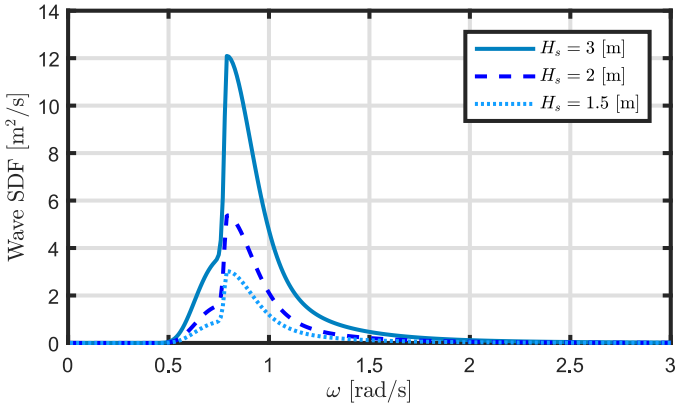

Fig. 5. JONSWAP spectra utilised to generate the wave inputs, with $T_p = 7.5$ [s], $H_s \in \{1.5, 2, 3\}$ [m] and $\gamma = 3.3$.

Table 1
Simulation results comparison table.

Model	Dim	NRMSE_F	NRMSE_T	T-Gain
Multi-SISO	72	0.76%	1.79%	(1.66×10^{-3})
$\tilde{\mathscr{H}}_{\mathscr{F}_1^{\text{sim}}}$	8	4.82%	13.77%	44.48%
$\tilde{\mathscr{H}}_{\mathscr{F}_2^{\text{sim}}}$	16	0.44%	1.78%	42.89%
$\tilde{\mathscr{H}}_{\mathscr{F}_3^{\text{sim}}}$	24	0.16%	0.65%	39.09%
$\tilde{\mathscr{H}}_{\mathscr{F}_4^{\text{sim}}}$	32	0.09%	0.34%	37.47%

sensible selection of the set $\mathscr{F}_1$, the moment-based approximating model, computed using a single interpolation point, already presents accurate results, though this performance is indeed improved by the set $\mathscr{F}_4$. Note that both parametric models have *exactly* the same response (both in magnitude and phase) as the target WEC array $H(j\omega)$, for each corresponding interpolation set $\mathscr{F}^{\text{sim}}$.

To provide a precise measure of the performance of the moment-

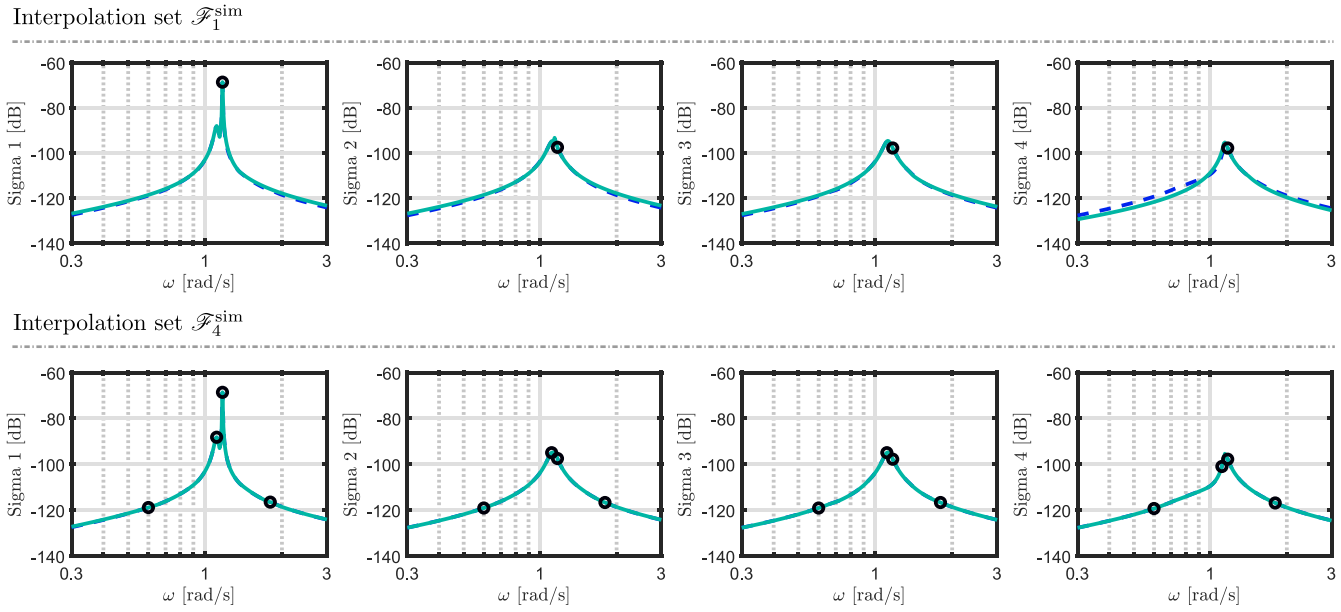

Fig. 6. Sigma-values plot (inputs 1 to 4) for both the target response $H(j\omega)$ (dashed-blue), and the approximating sigma mappings (solid-green) $\tilde{H}_{\mathscr{F}_1^{\text{sim}}}$ (top) and $\tilde{H}_{\mathscr{F}_4^{\text{sim}}}$ (bottom). The interpolation points are denoted by an empty black circle. (For interpretation of the references to color in this figure legend, the reader is referred to the web version of this article.)

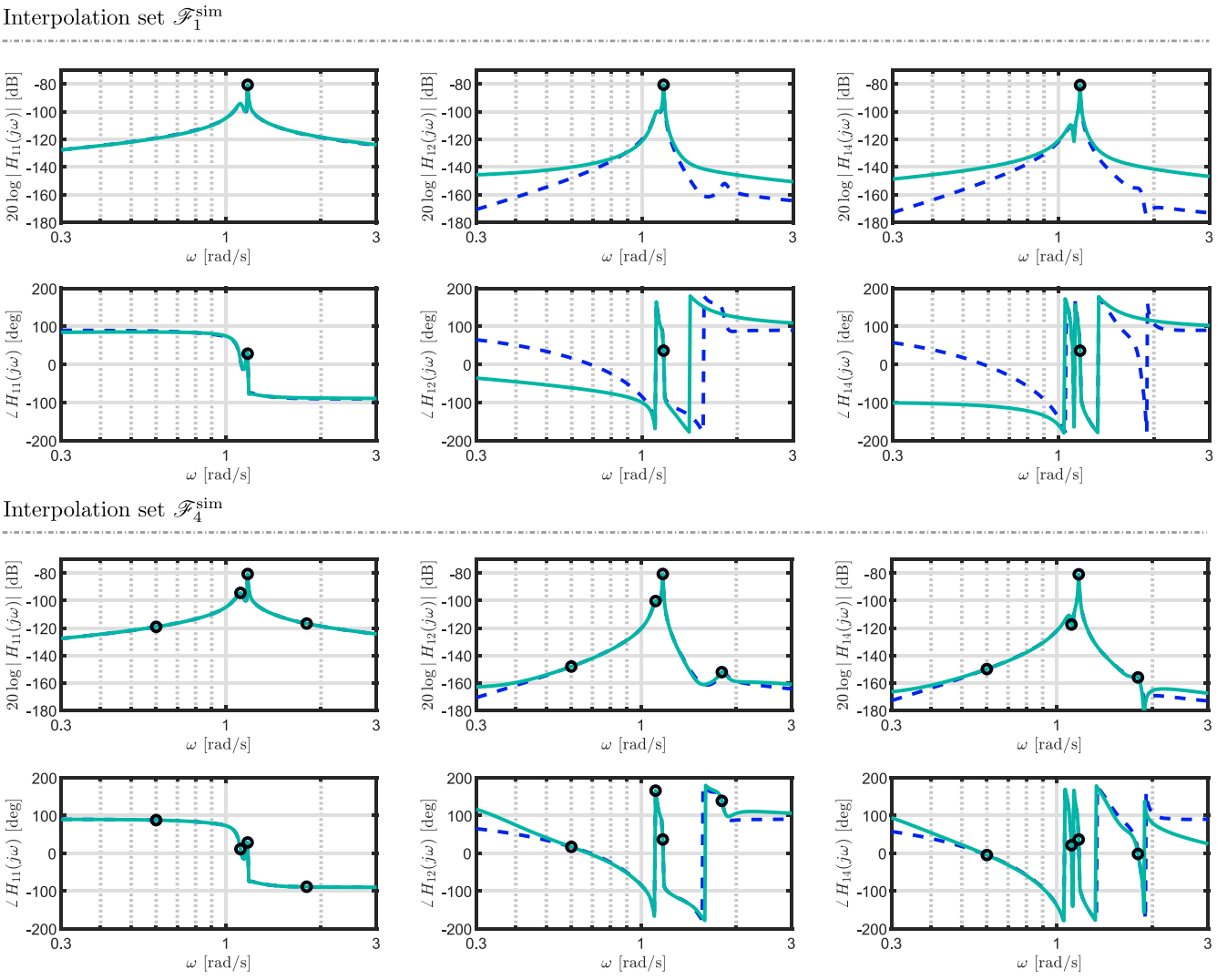

Fig. 7. Bode plots for the elements {1, 1}, {1, 2} and {1, 4}, for both the target response $H(j\omega)$ (dashed-blue), and the approximating frequency response mappings (solid-green) $\tilde{H}_{\mathscr{F}_1^{\text{sim}}}$ (top) and $\tilde{H}_{\mathscr{F}_4^{\text{sim}}}$ (bottom). The interpolation points are denoted by an empty black circle. (For interpretation of the references to color in this figure legend, the reader is referred to the web version of this article.)

based parametric approximations of the WEC array considered in this case study, Table 1 offers a numerical comparison in terms of the following key indicators:

- Dim Dimension (order) of the approximating parametric model.
- NRMSE_F Normalised Root Mean Square Error (NRMSE) computed against the target WEC array frequency response $H(j\omega)$, with $\omega \in \Omega$.
- NRMSE_T NRMSE computed (in steady-state) against the target time-domain response of the WEC array computed directly from $\mathscr{H}$ (*i.e.* explicitly solving each corresponding convolution integral associated with radiation effects). The corresponding wave excitation force inputs are computed from a JONSWAP spectrum with $H_s \in \{1.5, 2, 3\}$ [m], $T_p = 7.5$ [s] and $\gamma = 3.3$ (see Fig. 5).
- T-Gain % improvement in *normalised run-time* (*i.e.* the ratio between the time[13] required to compute one simulation, and the length of the simulation itself) with respect to the slowest model (normalised run-time indicated in table between parenthesis).

We note that the first row of Table 1 includes what we call the "multi-SISO" approach, which essentially constitutes a parametric model of the WEC array model $\mathscr{H}$ described in (19), obtained by approximating each individual convolution operator (arising due to hydrodynamic interaction between devices) with a SISO system, *i.e.* in a "decoupled" fashion. As discussed in Section 1, this is the predominant approach in the wave energy literature, and hence is included in Table 1 for the sake of comparison. In this paper, the strategy used to compute an approximation of each of these convolution terms separately, is the frequency-domain method presented in [42]. The dimension of each approximating model is set[14] to 4, which results in a full state-space description of the WEC array of dimension (order) 72.

It is straightforward to acknowledge, from Table 1, that the frequency-domain performance of the moment-matching based models is always over 95% accurate, being able to successfully represent the

[13] The computations are performed using MATLAB, running on a PC composed of an Intel Xeon CPU E5-1620 processor with 16 GB of RAM. The time is measured using the MATLAB embedded functions `Tic` and `Toc`.

[14] We note that the chosen dimension (four) corresponds to the average order considered to approximate radiation force subsystems among several studies, as discussed in [4].

target WEC array even in the case where a single interpolation frequency is (sensibly) chosen. In fact, it is noteworthy that the moment-matching based model $\tilde{\mathscr{H}}_{\mathscr{F}_1^{\text{sim}}}$ provides almost the same frequency response performance as the "multi-SISO" approach, but with $\approx$ 44% improvement in computational time (due to the substantial difference in model order). This performance is progressively improved by using the interpolation sets $\mathscr{F}_2^{\text{sim}}$, $\mathscr{F}_3^{\text{sim}}$ and $\mathscr{F}_4^{\text{sim}}$, with a mild increase in computational demand. In fact, the moment-based model with interpolation set $\mathscr{F}_2^{\text{sim}}$ already provides a better result than those of the "multi-SISO" approach, both in terms of accuracy and computational time. This is indeed directly associated with a sensible selection of the interpolation frequencies, as previously discussed in this same section.

Remark 15. It is certainly possible to improve the computational requirements of the "multi-SISO" approach, by subsequently applying a model order reduction technique. Naturally, this has some drawbacks: Firstly, the quality of the resulting (reduced) model directly depends on the first parameterisation stage, so that, for the non-parametric WEC case, the main focus should always be put in producing accurate models from the corresponding non-parametric data. Secondly, as expected from any model reduction technique, there is an intrinsic trade-off between improving the computational requirements of the model, and the final approximation quality.

The increase of approximation quality, when considering the different interpolation sets in time-domain simulations, is consistent with the previous frequency-domain results, though it can be appreciated that the approximating model $\tilde{\mathscr{H}}_{\mathscr{F}_1^{\text{sim}}}$ presents quite different behavior in the time- compared to the frequency- domain. This is due to the fact that the waves generated as inputs for this simulation scenario correspond to a JONSWAP spectrum with $T_p = 7.5[s]$, *i.e.* a peak frequency of $\approx$ 0.84 [rad/s]. As can be appreciated from Fig. 7, the fit between the frequency response of $\tilde{\mathscr{H}}_{\mathscr{F}_1^{\text{sim}}}$ and the target response of the WEC array is relatively poor in the neighborhood of 0.84 [rad/s], hence directly implying a loss of performance in this particular time-domain scenario.

Finally, to briefly illustrate the transient response of the approximating models computed with the presented strategy, Fig. 8 presents three different velocity curves, for a particular realisation with $H_s = 2$ [m]: Target steady-state response (dashed-blue), target transient response (dotted-blue), and transient response of the moment-matching-based model $\tilde{\mathscr{H}}_{\mathscr{F}_4^{\text{sim}}}$ (solid-green), for each of the devices composing the WEC array under analysis. The target transient response is computed by explicitly solving the convolution operation in (15). It can be readily noted that the velocity computed with the target and approximating model perfectly overlap throughout both the transient period (approximate length of 20 [s]), and the steady-state regime. We note that the transient response obtained with the "multi-SISO" approach behaves similarly to that of $\tilde{\mathscr{H}}_{\mathscr{F}_4^{\text{sim}}}$, and it is excluded from the plot for the sake of visibility.

6.2. Wave excitation force estimation

The estimation strategy considered in this paper is that utilised in [5], where the estimation of wave excitation force for a WEC array is discussed. This strategy belongs to the class of unknown input observers, where the system's input (wave excitation force $\mathscr{F}_e$ acting on the device) is estimated using only velocity measurements of the WEC array (*i.e.* the vector $\dot{\chi}(t)$) based on a direct application of the internal model principle [16]. To this end, a Kalman Filter (KF) [15] is used, in conjunction with a harmonic oscillator model, to describe the dynamics of the excitation force. In fact, we note that the dynamical model used to describe the excitation force is *exactly* defined by the signal generator proposed in (23). In other words, there is a natural synergy between the moment-matching-based parameterisation strategy proposed in this paper, and the unknown input estimation problem inherently present in wave energy systems.[15] This intrinsic connection, together with a summary of the unknown input estimation strategy presented in [5] (for the sake of completeness), are discussed in the subsequent paragraph.

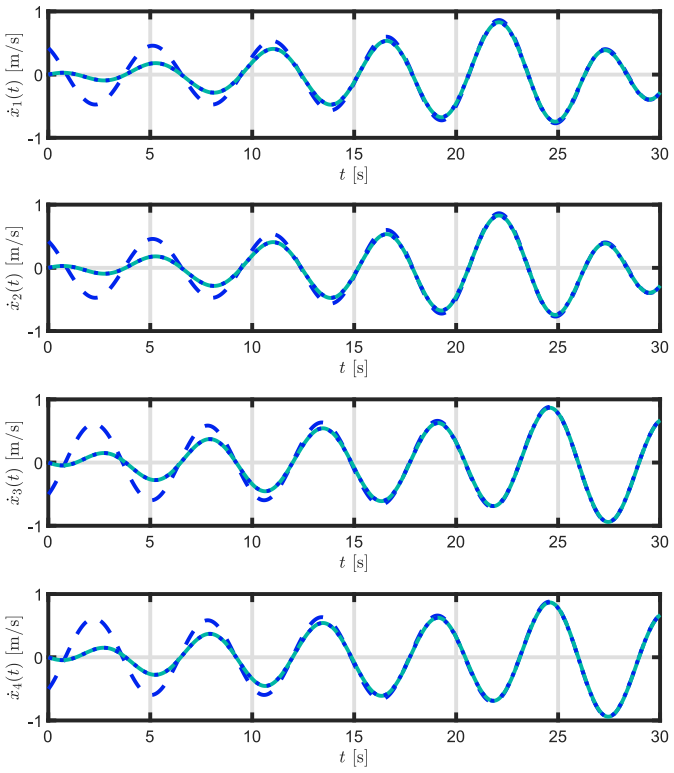

Fig. 8. Target steady-state response (dashed-blue), target transient response (dotted-blue), and transient response of the moment-matching-based model $\tilde{\mathscr{H}}_{\mathscr{F}_4^{\text{sim}}}$ (solid-green), for each of the devices composing the WEC array under analysis.. (For interpretation of the references to color in this figure legend, the reader is referred to the web version of this article.)

Table 2
Estimation results comparison table.

Model	Dim	Dim [e]	NRMSE_F	NRMSE_T [e]	T-Gain
Multi-SISO	72	88	0.76%	4.37%	(1.96×10^{-2})
$\tilde{\mathscr{H}}_{\mathscr{F}_1^{\text{sim}}}$	8	16	4.82%	23.59%	80.16%
$\tilde{\mathscr{H}}_{\mathscr{F}_1^{\text{est}}}$	8	16	31.12%	9.82%	80.16%
$\tilde{\mathscr{H}}_{\mathscr{F}_2^{\text{sim}}}$	16	24	0.44%	4.28%	68.92%
$\tilde{\mathscr{H}}_{\mathscr{F}_2^{\text{est}}}$	16	24	5.02%	2.04%	68.92%

With regard to the unknown input observer design, we begin by defining the so-called *augmented* system (see [16]), given by the following continuous-time system, described, for $t \in \mathbb{R}^+$, in state-space form as

$$\begin{aligned} \dot{\Upsilon} &= F_\text{a}\Upsilon + \epsilon, \\ \upsilon &= Q_\text{a}\Upsilon + \zeta, \end{aligned} \tag{34}$$

where $\epsilon(t)$ and $\zeta(t)$ represent the process and measurement (white) noises, with associated covariance matrices $\mathfrak{Q}_\epsilon$ and $\mathfrak{R}_\zeta$, respectively. The extended matrices, and state-vector, involved in (34), are defined as

[15] Note that, as reported in [14], the harmonic description of excitation forces has been exploited in several studies, using a variety of state observers.

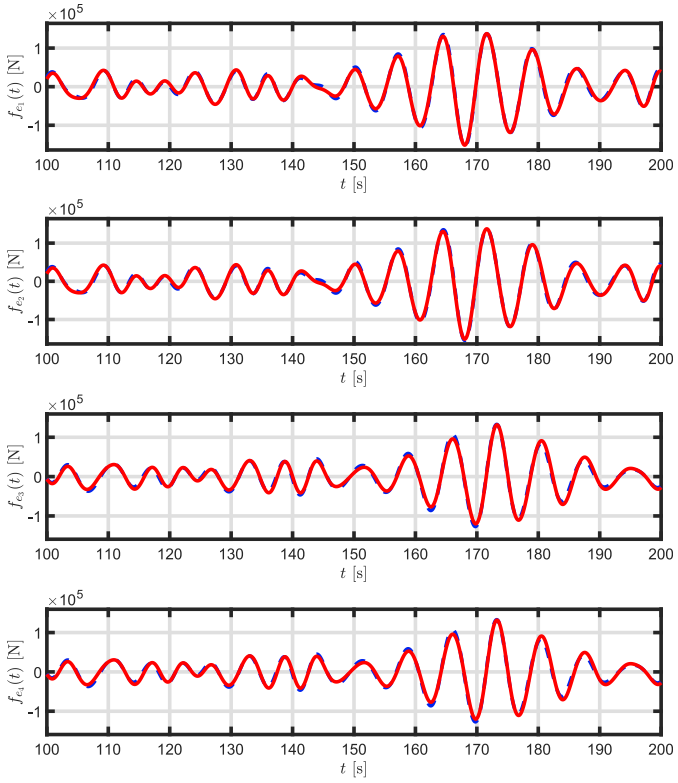

Fig. 9. Bode plots for the elements {1, 1}, {1, 2} and {1, 4}, for both the target response $H(j\omega)$ (dashed-blue), and the approximating frequency response mappings (solid-green) $\tilde{H}_{\mathscr{F}_1^{\text{sim}}}$ (top) and $\tilde{H}_{\mathscr{F}_1^{\text{est}}}$ (bottom). The interpolation points are denoted by an empty black circle. (For interpretation of the references to color in this figure legend, the reader is referred to the web version of this article.)

$$F_{\text{a}} = \begin{bmatrix} F_\varphi & G_\varphi^{\text{opt}} L_e \\ 0 & \mathbb{I}_N \otimes S \end{bmatrix}, \quad Q_{\text{a}} = [Q_\varphi \;\; 0],$$
$$\Upsilon = \begin{bmatrix} \Theta_\varphi \\ \Xi_e \end{bmatrix}, \tag{35}$$

where $\Upsilon(t) \in \mathbb{R}^{2N\nu}$ contains the system and signal generator state-vectors, *i.e.* $\Xi_e(t)$ and $\Theta_\varphi(t)$, respectively. Following [5], we define an optimal continuous-time KF observer as

$$\dot{\tilde{\Upsilon}} = F_{\text{a}}\tilde{\Upsilon} + \mathfrak{K}(y_\varphi - Q_{\text{a}}\tilde{\Upsilon}), \tag{36}$$

where the optimal gain $\mathfrak{K}\colon \mathbb{R}^+ \to \mathbb{R}$, $t \mapsto \mathfrak{K}(t)$, can be computed [15] as,

$$\begin{aligned} \dot{D} &= F_{\text{a}} D + D F_{\text{a}}^{\text{T}} - D Q_{\text{a}}^{\text{T}} \mathfrak{R}_\zeta^{-1} Q_{\text{a}} D + \Omega_\epsilon, \\ \mathfrak{K} &= D Q_{\text{a}}^{\text{T}} \mathfrak{R}^{-1}. \end{aligned} \tag{37}$$

Finally, the estimated wave excitation force can be directly computed in terms of the estimated state-vector as

$$\tilde{\mathscr{F}_e} = L_e [0 \;\; \mathbb{I}_{N\nu}] \tilde{\Upsilon}. \tag{38}$$

As can be directly appreciated from Eq. (35), F_{a} explicitly includes the dynamic matrix of the signal generator (23), which is utilised in the moment-based parameterisation method discussed in Section 5. We now show that this mathematical connection can be exploited to improve the performance of the unknown input observer substantially, by a wise selection of the set of interpolation points $\mathscr{F}$. To be precise, if we compute a parametric representation by moment-matching the input-output dynamics of the WEC array $\mathscr{H}_{\mathscr{F}}$, interpolating the same set of frequencies used to describe the internal model of the wave excitation force in the observer defined in (36) (*i.e.* the set $\lambda(S)$), the performance of the unknown input estimator improves when compared to the case where the currently most-used parameterisation approach (*i.e.* "multi-SISO") is considered to describe the WEC array motion. This is associated with the fact that the model based on the moment-matching strategy presented herein has *exactly* the same steady-state response as the target non-parametric model of the WEC array computed with BEM solvers at the key frequencies utilised to describe the excitation input. We note that this improvement in performance is given both in terms of estimation quality and computational effort required by the observer, as demonstrated in the remainder of this section.

To illustrate the advantages of using the moment-based parameterisation method proposed in this paper within the unknown input estimation problem, we design a KF observer with a matrix S completely characterised by the sets (see Eq. (24)):

$$\begin{aligned} \mathscr{F}_1^{\text{est}} &= \{0.84\}, \\ \mathscr{F}_2^{\text{est}} &= \{0.84,\ 1.17\}. \end{aligned} \tag{39}$$

where we note that $\mathscr{F}_1^{\text{est}} \subset \mathscr{F}_2^{\text{est}}$. The definition of the set $\mathscr{F}_1^{\text{est}}$ is made using explicit knowledge of the stochastic description of the wave excitation force input: a key frequency to take into account in the internal model description is that characterising the peak of the JONSWAP spectrum of Fig. 5, *i.e.* $2\pi/7.5 \approx 0.84$ [rad/s]. The second set includes the frequency point 1.17 [rad/s] which, as discussed previously in Section 6.1, characterises the $\mathscr{H}_\infty$-norm of the WEC array.[16] Using the frequency sets defined in Eq. (39), we compute the moment-based state-space models $\tilde{\mathscr{H}}_{\mathscr{F}_1^{\text{est}}}$ and $\tilde{\mathscr{H}}_{\mathscr{F}_2^{\text{est}}}$ following the procedure described in Algorithm 1.

Considering these two moment-based models, specifically designed to correlate with the optimal observer of Eq. (36), and the moment-matching models $\tilde{\mathscr{H}}_{\mathscr{F}_1^{\text{sim}}}$ and $\tilde{\mathscr{H}}_{\mathscr{F}_2^{\text{sim}}}$, computed for the WEC array motion simulation case of Section 6.1, we design a KF using each of the parametric representations listed above, and assess the performance of the different unknown input observers in terms of the following indicators. Note that, analogously to Section 6.1, we also include in the upcoming discussion a KF designed using the state-space model arising from the "multi-SISO" model.

- Dim — Dimension (order) of the approximating parametric model describing the WEC dynamics.
- Dim $^{\text{e}}$ — Dimension (order) of the wave excitation force estimator.
- NRMSE_{F} — NRMSE of the parametric model approximating the WEC array dynamics computed against the target WEC array frequency response $H(j\omega)$, with $\omega \in \Omega$.
- NRMSE_{T} $^{\text{e}}$ — NRMSE computed (in steady-state) against the target wave excitation force signal, computed from a JONSWAP spectrum with $H_s \in \{1.5, 2, 3\}$ [m], $T_p = 7.5$ [s] and $\gamma = 3.3$ (see Fig. 5).
- T-Gain — % improvement in *normalised run-time* (*i.e.* the ratio between the time required to compute the estimated wave excitation force, and the length of the simulation itself) with respect to the slowest model (normalised run-time indicated in table between parenthesis).

We begin the analysis of Table 2 by making an explicit performance comparison between the moment-matching-based models $\tilde{\mathscr{H}}_{\mathscr{F}_1^{\text{sim}}}$ and $\tilde{\mathscr{H}}_{\mathscr{F}_1^{\text{est}}}$, for the unknown input estimation problem. Note that the dimension (order) of both models is exactly the same, *i.e.* the same number of interpolation points are used to compute both parametric representations. Despite sharing the same model complexity, the performance results are significantly different, as discussed in the following.

Whilst $\tilde{\mathscr{H}}_{\mathscr{F}_1^{\text{sim}}}$ provides a much better overall approximation in

[16] We refer the reader to [5,14] for further discussion on the selection of the frequency points to represent stochastic wave excitation forces using the internal model principle.

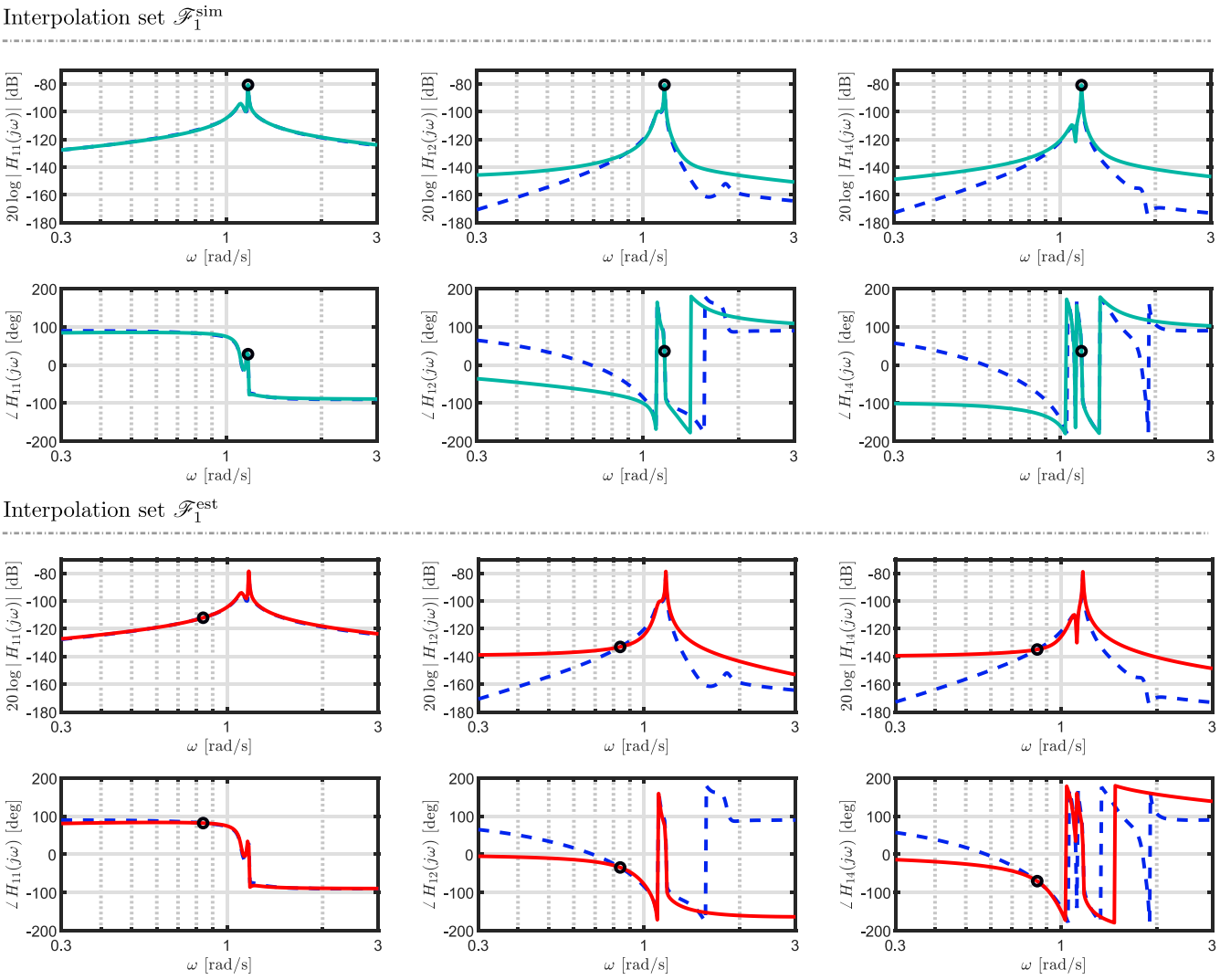

Fig. 10. Target (dashed-blue) and estimated (solid-red) wave excitation forces for each device in the WEC array, using a KF designed with the moment-based parametric model $\tilde{\mathscr{H}}_{\mathscr{F}_1^{\text{est}}}$. (For interpretation of the references to color in this figure legend, the reader is referred to the web version of this article.)

frequency-domain (with almost 96% of accuracy) than $\tilde{\mathscr{H}}_{\mathscr{F}_1^{\text{est}}}$, the performance of the estimator designed using $\tilde{\mathscr{H}}_{\mathscr{F}_1^{\text{sim}}}$ is quite poor, with a NRMSE_{T} [e] of $\approx$ 24%. Instead, having a frequency-domain NRMSE_{F} of almost 32%, the KF designed used $\tilde{\mathscr{H}}_{\mathscr{F}_1^{\text{est}}}$ performs substantially better in terms of wave excitation force estimation quality, with less than 10% of estimation error. This can be attributed to the fact that $\tilde{\mathscr{H}}_{\mathscr{F}_1^{\text{est}}}$ has *exactly* the same steady-state response as the WEC array at the frequency points selected to represent the internal model of the excitation force embedded in the optimal observer (36), where the majority of the spectral content of the input signal is contained (see Fig. 5). Fig. 9 graphically illustrates the performance of the KF designed using $\tilde{\mathscr{H}}_{\mathscr{F}_1^{\text{est}}}$ for a time-window of 100 [s], where it can be appreciated that both time traces, *i.e.* target (dashed-blue) and estimated (solid-red) wave excitation forces, for each of the four devices composing the analysed WEC array, are qualitatively identical.

Fig. 10 shows a Bode diagram analogous to that of Fig. 7, where the frequency-domain description and performance of the parametric models $\tilde{\mathscr{H}}_{\mathscr{F}_1^{\text{sim}}}$ and $\tilde{\mathscr{H}}_{\mathscr{F}_1^{\text{est}}}$ can be explicitly appreciated. Note that, consistent with the results of Table 2, the overall frequency-domain fit for the selected frequency range of $\tilde{\mathscr{H}}_{\mathscr{F}_1^{\text{sim}}}$ is clearly better than $\tilde{\mathscr{H}}_{\mathscr{F}_1^{\text{est}}}$, though $\tilde{\mathscr{H}}_{\mathscr{F}_1^{\text{est}}}$ interpolates in a key frequency point for the unknown input estimation problem, thus significantly improving the performance of the corresponding KF.

It is noteworthy to highlight that exploiting this inherent relation between moment-matching parameterisation and the internal model principle, used to estimate the wave excitation force, using a single interpolation point $\mathscr{F}_1^{\text{est}}$, provides similar estimation accuracy results as the case where the "multi-SISO" approach is considered, but with $\approx$ 81% improvement in computational requirements. In other words, the estimator using the moment-based model $\tilde{\mathscr{H}}_{\mathscr{F}_1^{\text{est}}}$ computes 81% faster than the currently most-used method, for the same degree of wave excitation force estimation accuracy, and is therefore especially suited for real-time applications.

Finally, Table 2 also provides results for the KF observers designed using the moment-based models $\tilde{\mathscr{H}}_{\mathscr{F}_2^{\text{sim}}}$ and $\tilde{\mathscr{H}}_{\mathscr{F}_2^{\text{est}}}$, where the perfomance (frequency-domain fitting and wave excitation force estimation quality) is subsequently improved, for both cases. Note that the situation described in the previous paragraph is repeated, *i.e.* the KF designed using $\tilde{\mathscr{H}}_{\mathscr{F}_2^{\text{est}}}$ provides better estimation performance due to the particular selection of the interpolation points (same as those carefully selected to describe the internal model of the input in (36)).

7. Conclusions

In this paper, we present a MIMO moment-based parameterisation strategy for wave energy applications, making specific emphasis in motion simulation and wave excitation force estimation. This approach allows for the computation of state-space representation characterising

the input-output dynamics of WEC arrays which *exactly* matches the target steady-state behavior of the array at a set of user-selected frequencies. We explicitly discuss how the selection of these interpolation points have a key role in the performance of the computed models, both for WEC array motion simulation and wave excitation force estimation applications. In fact, we show that there exists an intrinsic mathematical relation between the unknown input wave excitation force estimation problem and the moment-based strategy presented herein, which we exploit by a sensible selection of the set of interpolation points, in synergy with the internal model principle utilised to estimate $\mathscr{F}_e$. Finally, we analyse the performance of the strategy using a state-of-the-art WEC array composed of CorPower-like devices, showing that we can outperform the "multi-SISO approach" (*i.e.* currently used method) both in terms of accuracy and computational requirements, hence providing models that are especially suited to design real-time energy-maximisiation strategies, contributing to the roadmap towards successful commercialisation of WEC devices.

CRediT authorship contribution statement

Nicolás Faedo: Conceptualization, Methodology, Formal analysis, Investigation, Writing - original draft. **Yerai Peña-Sanchez:** Software, Methodology, Validation, Visualization, Writing - review & editing. **John V. Ringwood:** Conceptualization, Supervision, Project administration, Funding acquisition, Writing - review & editing.

Declaration of Competing Interest

The authors declare that they have no known competing financial interests or personal relationships that could have appeared to influence the work reported in this paper.

Acknowledgment

The authors would like to acknowledge Prof. Alessandro Astolfi and Dr. Giordano Scarciotti from Imperial College London for useful discussions on moment-based theory. This material is based upon works supported by Science Foundation Ireland under grant no. 13/IA/1886.

References

Cruz, J., 2008. Ocean Wave Energy: Current Status and Future Perspectives. Springer Science & Business Media.
Ruehl, K., Bull, D., 2012. Wave energy development roadmap: design to commercialization. 2012 Oceans. IEEE, pp. 1–10.
Folley, M., 2016. Numerical Modelling of Wave Energy Converters: State-of-the-Art Techniques for Single Devices and Arrays. Academic Press.
Faedo, N., Olaya, S., Ringwood, J.V., 2017. Optimal control, MPC and MPC-like algorithms for wave energy systems: An overview. IFAC J. Syst. Control 1, 37–56.
Peña-Sanchez, Y., Garcia-Abril, M., Paparella, F., Ringwood, J.V., 2018. Estimation and forecasting of excitation force for arrays of wave energy devices. IEEE Trans. Sustain. Energy 9 (4), 1672–1680.
Babarit, A., Delhommeau, G., 2015. Theoretical and numerical aspects of the open source BEM solver NEMOH. 11th European Wave and Tidal Energy Conference, Nantes.
Cummins, W., 1962. The impulse response function and ship motions. Schiffstechnik 47, 101–109.
Ogilvie, T.F., 1964. Recent progress toward the understanding and prediction of ship motions. 5th Symposium on Naval Hydrodynamics, Bergen, Norway. 1. pp. 2–5.
Wazwaz, A.-M., 2011. Volterra integro-differential equations. Linear and Nonlinear Integral Equations. Springer, pp. 175–212.
Pavel, K., David, S., 2013. Algorithms for efficient computation of convolution. Des. Archit. Digit. Signal Process. 179–208. https://doi.org/10.5772/51942.
Zou, S., Abdelkhalik, O., 2019. Consensus estimation in arrays of wave energy converters. IEEE Trans. Sustain. Energy 10 (2), 943–951.
Zhong, Q., Yeung, R.W., 2019. Model-predictive control strategy for an array of wave-energy converters. J. Mar. Sci. Appl. 1–12.
Faedo, N., Scarciotti, G., Astolfi, A., Ringwood, J.V., 2019. Moment-based constrained optimal control of an array of wave energy converters. 2019 American Control Conference (ACC), Philadelphia. pp. 4797–4802.
Peña-Sanchez, Y., Windt, C., Davidson, J., Ringwood, J.V., 2019. A critical comparison of excitation force estimators for wave energy devices. IEEE Control Syst. Technol. (early access available)
Simon, D., 2006. Optimal State Estimation: Kalman, H_∞, and Nonlinear Approaches. John Wiley & Sons.
Francis, B.A., Wonham, W.M., 1976. The internal model principle of control theory. Automatica 12 (5), 457–465.
Faedo, N., Peña-Sanchez, Y., Ringwood, J.V., 2018. Finite-order hydrodynamic model determination for wave energy applications using moment-matching. Ocean Eng. 163, 251–263.
Peña-Sanchez, Y., Faedo, N., Ringwood, J.V., 2019. Moment-based parametric identification of arrays of wave energy converters. 2019 American Control Conference (ACC), Philadelphia. pp. 4785–4790.
CORPOWER ocean, (http://www.corpowerocean.com/), Accessed: 2019-05-17.
Brewer, J., 1978. Kronecker products and matrix calculus in system theory. IEEE Trans. Circuits Syst. 25 (9), 772–781.
Astolfi, A., 2010. Model reduction by moment matching for linear and nonlinear systems. IEEE Trans. Autom. Control 55 (10), 2321–2336.
Scarciotti, G., Astolfi, A., 2017. Nonlinear model reduction by moment matching. Found. Trends Syst. Control 4 (3–4), 224–409.
Scarciotti, G., 2017. Low computational complexity model reduction of power systems with preservation of physical characteristics. IEEE Trans. Power Syst. 32 (1), 743–752.
Antoulas, A.C., 2005. Approximation of Large-Scale Dynamical Systems. SIAM.
Isidori, A., 2013. Nonlinear Control Systems. Springer Science & Business Media.
Padoan, A., Scarciotti, G., Astolfi, A., 2017. A geometric characterization of the persistence of excitation condition for the solutions of autonomous systems. IEEE Trans. Autom. Control 62 (11), 5666–5677.
Li, G., Belmont, M.R., 2014. Model predictive control of sea wave energy converters–part II: the case of an array of devices. Renew Energy 68, 540–549.
Zhong, Q., Yeung, R.W., 2018. Performance of a wave-energy-converter array operating under model-predictive control based on a convex formulation. ASME 2018 37th International Conference on Ocean, Offshore and Arctic Engineering. American Society of Mechanical Engineers. V009T13A038–V009T13A038
Falnes, J., 2002. Ocean Waves and Oscillating Systems: Linear Interactions Including Wave-Energy Extraction. Cambridge university press.
Ringwood, J.V., Mérigaud, A., Faedo, N., Fusco, F., 2019. An analytical and numerical sensitivity and robustness analysis of wave energy control systems. IEEE Trans. Control Syst. Technol. 1–12. (early access)
Wolfram, J., 1999. On alternative approaches to linearization and Morison's equation for wave forces. Proc. R. Soc. Lond. Ser. A 455 (1988), 2957–2974.
Faedo, N., Peña-Sanchez, Y., Ringwood, J.V., 2019. Moment-matching-based input-output parametric approximation for a multi-DoF wec including hydrodynamic nonlinearities. 13th European Wave and Tidal Energy Conference, Naples. 1449–1–1449–10
Penalba, M., Kelly, T., Ringwood, J.V., 2017. Using NEMOH for modelling wave energy converters: Acomparative study with WAMIT. 12th European Wave and Tidal Energy Conference, Cork. 631–1–631–10
McKelvey, T., Akçay, H., Ljung, L., 1996. Subspace-based multivariable system identification from frequency response data. IEEE Trans. Autom. Control 41 (7), 960–979.
Boyd, S., Vandenberghe, L., 2004. Convex Optimization. Cambridge University Press.
Giorgi, G., Ringwood, J.V., 2018. Analytical representation of nonlinear Froude-Krylov forces for 3-DoF point absorbing wave energy devices. Ocean Eng. 164, 749–759.
Todalshaug, J.H., Ásgeirsson, G.S., Hjálmarsson, E., Maillet, J., Möller, P., Pires, P., Guérinel, M., Lopes, M., 2016. Tank testing of an inherently phase-controlled wave energy converter. Int. J. Mar. Energy 15, 68–84.
Folley, M., Forehand, D., 2016. Chapter 8 - conventional multiple degree-of-freedom array models. In: Folley, M. (Ed.), Numerical Modelling of Wave Energy Converters. Academic Press, pp. 151–164.
Hasselmann, K., 1973. Measurements of wind wave growth and swell decay during the Joint North Sea Wave Project (JONSWAP). Dtsch. Hydrogr. Z. 8, 95.
Mérigaud, A., Ringwood, J.V., 2017. Free-surface time-series generation for wave energy applications. IEEE J. Oceanic Eng. 43 (1), 19–35.
Zhou, K., Doyle, J.C., 1998. Essentials of robust control. 104 Prentice hall, Upper Saddle River, NJ.
Perez, T., Fossen, T.I., 2009. A Matlab toolbox for parametric identification of radiation-force models of ships and offshore structures. Model. Identif. Control 30 (1), 1–15.